Instruments for Neutron Scattering

Michael Monkenbusch

This document has been published in

Manuel Angst, Thomas Brückel, Dieter Richter, Reiner Zorn (Eds.):
Scattering Methods for Condensed Matter Research: Towards Novel Applications at Future Sources
Lecture Notes of the 43rd IFF Spring School 2012
Schriften des Forschungszentrums Jülich / Reihe Schlüsseltechnologien / Key Technologies, Vol. 33
JCNS, PGI, ICS, IAS
Forschungszentrum Jülich GmbH, JCNS, PGI, ICS, IAS, 2012
ISBN: 978-3-89336-759-7

C 3 Instruments for Neutron Scattering

Michael Monkenbusch
Jülich Center for Neutron Science
Forschungszentrum Jülich, D-52425 Jülich

Contents

1 Introduction

In general [1] a neutron scattering instrument measures the double differential cross section

$$\frac{d^2\sigma}{d\Omega dE'} \;=\; N\,\frac{k'}{k} b^2 S(\mathbf{Q},\omega) \tag{1}$$

where k', k denote the wavevector lengths of the scattered (k') and the incoming neutrons. For a simple monoatomic bulk sample N is the number atoms and b their scattering length. The available physical information may be expressed in terms of the scattering function $S(\mathbf{Q},\omega)$. The energy transfer that occurs during the scattering process $\hbar\omega = (E - E')$ is given by the difference of the energy E of incoming and scattered neutrons (E'). The momentum transfer $\hbar Q$ is proportional to the difference $\mathbf{Q} = \mathbf{k} - \mathbf{k}'$ of initial and final wavevectors. Also the energy transfer is related to the change in these wavevectors

$$\hbar\omega = (\hbar^2/2m_n)(k^2 - k'^2) \tag{2}$$

according to the relation between $\mathbf{k}$ and the neutron velocity $\mathbf{v}$ and neutron wavelength λ

$$\mathbf{v}m_n \;=\; \hbar\mathbf{k} \quad \text{and} \quad \frac{2\pi}{\lambda} \;=\; k \tag{3}$$

The energy transfer may be obtained either by direct neutron velocity measurements using their flight times or –using the wave properties– by analysis of the wavelength by e.g. Bragg reflection from a periodic structure (crystal, multilayer). Instruments as diffractometers that focus on the microscopic structure of the sample mainly analyze the $\mathbf{Q}$ dependence of the scattering without energy analysis. The same is true for reflectometers. On the other hand spectrometers focus on the energy transfer $\hbar\omega$ during scattering and its dependence on the momentum transfer $\mathbf{Q}$.

Depending on the application and the abilities of the used techniques as well $\hbar\omega$ as $\mathbf{Q}$ are more or less precisely defined. The different combination of *resolutions* with respect to $\mathbf{Q}$ and ω yields the variety of instruments, in particular since the realized resolutions determine the maximum available intensity. Neutron scattering always is an intensity limited method, even for the most powerful research reactors or spallation sources. Thermal or cold neutrons emerge from a moderator which exposes an extended area (some $100\,\mathrm{cm}^2$) emitting neutrons in all direction and with a velocity distribution according to the effective moderator temperature. Therefore a good adaption of resolution of an instrument to the requirements of the physical question such that all acceptable neutrons from the source are utilized is a key to perform an experiment with optimum intensity on the detector.

Neutrons are spin 1/2 particles with an associated magnetic moment. The scattering cross sections of a sample may depend on the spin state of the incoming neutrons and the scattering may change the spin state. In particular samples with magnetic structures will show these kinds of polarization dependent scattering and analysis of it can reveal details on magnetic structures and excitations.

[1] Note that the majority of neutron instruments at reactor or spallation sources are scattering instruments including reflectometers. However, there are also some other applications as radiographic and tomographic imaging or the study of nuclear reactions due to neutron capture for chemical analysis or nuclear physics experiments. Finally some fundamental physics apparatus are devoted to the properties of the neutron itself as e.g. precise measurement of it's lifetime or the search for an electrical dipole moment. These are not covered by the present article.

In the following of this chapter a selection the most important instrument types to investigate structures in condensed matter samples are presented. These *diffractometers*, which do not analyze the energy transfer but detect all neutrons that are scattered by the sample, are explained. The structure information is obtained from the scattering angle or more precise the $\mathbf{Q}$ dependence of the intensity. The implicit diffractometer assumption in general is that there is only negligible or no energy transfer.
Later *spectrometers* that focus on the analysis of the energy transfer during scattering are described. Here motion and motional patterns on atomic scale or excitations are addressed. Depending on the instrument the $\mathbf{Q}$ resolution is worse than those of a diffractometer in order to collect sufficient intensity to enable the spectral analysis. The covered energy transfers (not by a single instrument) range from 10% down to 0.1% of the initial neutron energy for instruments with direct spectral analysis, e.g. by Bragg reflection, and further down into the ppm regime for neutron-spin-echo spectrometers.
First the most important functional components that are part of neutron scattering instruments are now presented.

2 Components

2.1 Divergence Control

Neutron sources with sufficient intensity for scattering instrumentation are either research reactors or spallation sources. Neutrons with suitable wavelength for scattering experiments on condensed matter are obtained by down-scattering and thermalization in a moderator (see chapter C1). The moderators emit a spectrum with broad energy spread of neutrons, which is close to a Maxwell distribution corresponding to the effective temperature plus a contribution of so-called epithermal neutrons that still are not fully slowed down. The neutrons emerge from an extended area (surface of the moderator). The moderator emits neutrons without preferred direction.
Instruments receive the neutrons through channels in the several meters thick radiation shielding leading to the moderators. They have typical cross sections of $\simeq 10 \cdots 20\,\mathrm{cm}$ and several m length. In order to obtain a suitably well defined wavevector, neutrons of a certain direction have to be selected. A process called collimation (see fig. 1). The simplest way would be to rely on entrance an exit apertures (“pin-holes”) in a certain distance. And in a way the channel in the shielding may serve as a coarse collimator. If however this it not sufficient other types of collimation, in particular Soller collimators [1] are used. These collimators consist of an array of parallel absorbing sheets in a frame. Only a few isotopes are available to realize effective absorbers from which pin-holes, diaphragms aperture blades and collimator sheets can be made. For thermal and cold neutrons these parts preferentially contain $^{10}\mathrm{B}$, Gd or Cd and eventually $^{6}\mathrm{Li}$. Here material thicknesses in the range from a tenth to a few mm usually suffice. A good collimation yields a narrow spread of neutron directions in the beam on the expense of intensity. If space around a neutron source has to be shared by many instruments or if for a pulsed source a certain distance is required for a time-of-flight tagging of the neutron velocity, a large distance between source (moderator) and sample often will result. In most of these cases the “natural” collimation that results from the ratio of moderator(opening) plus sample sizes compared to their distance is much narrower than the instrument requires. To avoid the intensity loss due to this mismatch of beam divergence so-called *neutron guides* are used to bridge the

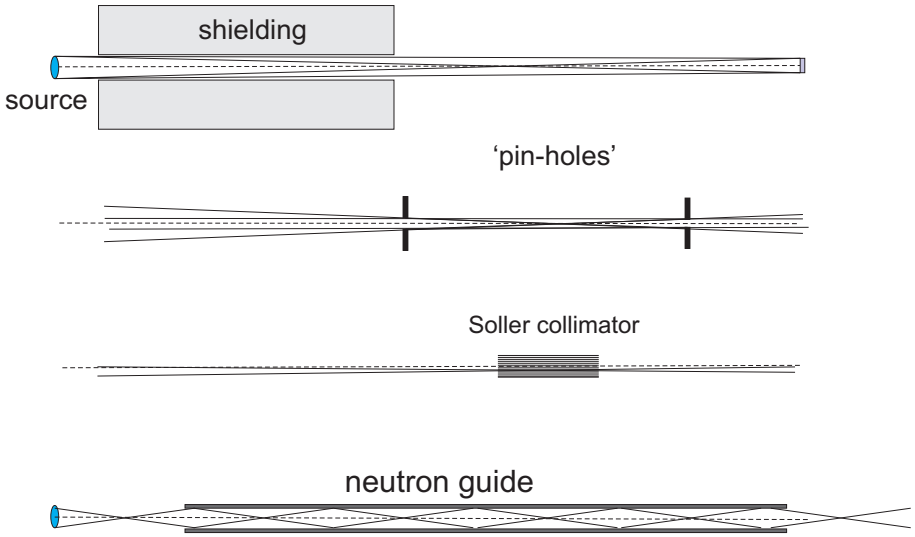

Fig. 1: *The divergence of a neutron beam is naturally limited by the effective source size or the beam channel width, the sample (target) size and their distance. Explicit control can be obtained by pin-holes, diaphragms or slits at a distance, in those cases the beam diameter and the degree of collimation determines the required length. Finally compact Soller collimators with many parallel (or radially converging) channels decouple length, beam width and achieved divergence. Finally neutron guides (channels with reflecting surface, see text) are used if the natural divergence would be to small.*

distance. Neutron guides consist of evacuated (rectangular) channels with very smooth coated inner surfaces. The coating is such that neutrons that hit the surface at a sufficiently flat angle are reflected. For most elements the effective index of refraction, $n = 1 - \lambda^2\, b\, N/(2\pi)$ (with b=scattering length and N=number density of nuclei) for thermal neutrons is less than 1. This means that below a limit angle of incidence neutrons undergo total reflection at a polished surface of such an element. The standard coating that utilizes total reflection is a layer of several 100nm of Ni, the angle of total reflection may be increased by 20% if $^{58}\mathrm{Ni}$ is used instead of natural Ni. Even larger reflection angles are realized by multilayer coatings as Ni/Ti. The ratio of the maximum reflection angle of a given (multi)layer and a standard Ni coating usually is denoted by $\mathbf{m}$. Guides with **m**-values between 2 and 3 are readily available 5-6 seems technical feasible. However, the required number of layers, i.e. the effort and cost increases steeply with m. For a given layer the maximum reflection angle is proportional to the neutron wavelength and the value is about 1^0 for $10\,\text{Å}$ neutrons for a Ni coating.

2.2 Spectrum Control

Besides the direction selection a well defined initial wavevector in addition requires the selection of a specific neutron wavelength, i.e. neutron velocity. The method employed in the first neutron instruments and which still is widely used for this purpose is the Bragg reflection by large (mosaic) crystals. Nowadays widely used are pyrolytic graphite, PG(002), Si(111,311), Cu(111,200,220,331), Ge(hhl) and for polarization Heusler alloy $\mathrm{Cu_2\,Mn\,Al}$(111) crystals. Since the primary neutrons have a continuous wavelength distribution the intensity of the reflected beam is proportional to the width of the selection band. A very perfect crystal

yields a well defined selection, however, with little intensity. Therefore for many applications in neutron scattering imperfect crystals with a "mosaic" of small slightly misaligned domains are preferred or even essential. Whereas for Si special effort and skill is needed to "deteriorate" the available nearly perfect crystals in a defined manner into a mosaic crystal, for pyrolytic graphite the manufacturing process rather yields crystals at the other margin of perfection. For most purposes where cold neutrons with about 1% wavelength definition are needed graphite is the first choice. For shorter wavelength neutrons e.g. germanium or copper crystals may be used. See figure 2.
Depending on application the selected wavelength λ may be contaminated by intensity from higher order reflection $\lambda/2,\ \lambda/3, \cdots$. In those cases additional filters are needed that are based on crystalline Bragg reflection (e.g. Be-filter [2]) or a mechanical velocity selector [3, 4].

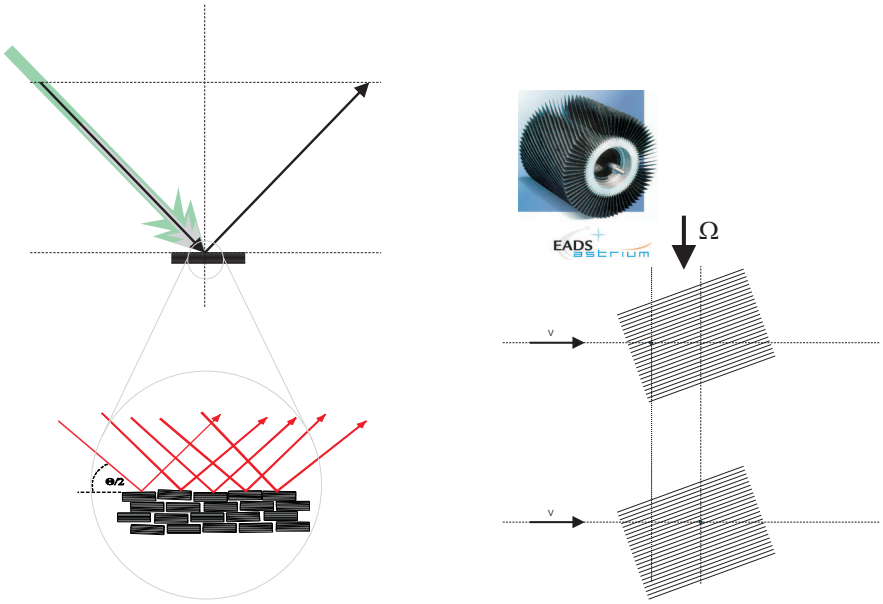

Fig. 2: *A suitable means to select a narrow wavelength respectively velocity band from a "white" beam of neutrons is: left:the Bragg reflection from a crystal. Suitable crystals are e.g. Graphite (002), Copper, Germanium etc.. Or right: a mechanical velocity selector. A inclined collimating structure, usually helically wound lamellae on the periphery of a rotating cylinder move perpendicular to the beam direction. A certain open channel section along the beam axis therefore moves with a velocity* $v = v_r / \tan\alpha = \Omega\, r / \tan\alpha$*, with* α *the inclination angle,* v_r *the velocity of the cylinder periphery at radius* r*.*

But not only the wave property of the neutron allows a selection of wavelength. Since the wavelength is proportional to the velocity and the typical neutron velocities range between several 100 m/s to a few 1000 m/s it may also be chosen by controlling the neutron time-of-flight over a distance of a few meters. This can be achieved by means of choppers that open the neutron beam path periodically for a short time. The delay between different choppers along a beam path thus determines the velocity of the transmitted neutron bunches. Disc choppers consist of a rotating absorbing disc with neutron transparent sectors and rotating axis parallel to the beam direction. So called Fermi-choppers [5] on the other hand are small rotating collimators that for a short period of their revolution are aligned with the beam direction. The rotation axis is perpendicular to the beam direction. Disc choppers need some time to switch a larger beam

cross section from closed to open whereas Fermi-choppers may do this in a shorter time. However, their collimation direction changes at a high rate and thus slow neutrons may be hit by an absorbing wall before they leave the chopper again. This effect may be utilized to select a limited velocity band by bending the collimation channels.
Even more this effect is used in mechanical velocity selectors (figure 2), where absorbing lamellae in a twisted configuration are on the periphery of a rotating cylinder. If the neutron velocity matches the apparent speed of the gap between two lamellae on a path parallel to the rotation axis, the neutron is transmitted without being hit by an absorbing wall. Neutrons with differing velocities are absorbed. Unlike a chopper the velocity selector performs a coarse monochromatization for a continuous beam. Typical monochromatizations are about 10% of the mean velocity.

2.3 Polarization

The first methods used to prepare and analyze polarized neutron beams rely on the magnetic part of Bragg reflections [6, 7] including the use of magnetized polycrystalline iron as polarizing filter. Today Heusler crystals of the type $\mathrm{Cu_2\,Mn\,Al}$ are used as efficient polarizing monochromators for thermal neutrons. Cold neutrons rather are polarized by utilizing the spin dependent reflection from magnetic multilayers, as illustrated in figure 3 . Common A-B multilayer systems are FeCo-Ti and Fe-Si [8], the choice is made such that the contrast between the magnetized A and the nonmagnetic B layer vanishes for one spin state and has a sizable value for the other. Only neutrons with spin states that "see" the contrasts are reflected by the multilayer stack. The layer thickness is varied over the stack such that reflection is large over a wide range of incident angles respectively wavelengths up to a maximum. The maximum value is specified in terms of multiples m of the total reflection edge of Ni. m values up to and even beyond $m = 4$ are state of the art.

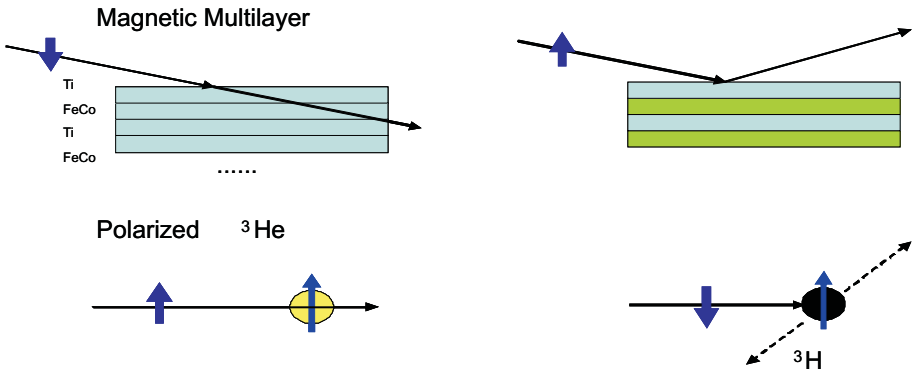

Fig. 3: *Illustration of two important techniques to polarize neutron beams. Upper part: layering of a magnetic and nonmagnetic material with layer distances in the several nm range is used to yield a reflecting structure for one spin component. The neutron spin interaction with the magnetization adds or subtracts to the nuclear potential and is adjusted such that for one spin state the layering becomes invisible. Bottom: an alternative way to polarize neutrons is to utilize the fact that the absorption of neutrons by ^{3}He is spin dependent. Here the challenge is to establish and preserve a high nuclear polarization of the ^{3}He nuclei.*

Finally neutrons may be polarized by absorption from nuclear spin polarized ^{3}He. The high

absorption cross section of ^{3}He holds only for one spin state. The absorption cross section is proportional to the neutron wavelength. Special quartz cells containing spin-polarized ^{3}He at pressures close to 1 bar can be position in the neutron path as polarization filters. The advantage of a polarized ^{3}He filter is its wide angular acceptance even for short wavelengths. The technical difficulty consists in creating and maintaining the polarization of ^{3}He nuclei either off-line (MEOP) [9] or on-line in a steady state setup (SEOP) [10]. Preservation of ^{3}He polarization requires a very homogeneous magnetic field and selected cells with low magnetic impurities exposed by the inner wall. Since the maximum nuclear polarization is significantly less than 100% and in off-line cells decays with time constants of a few 100h the thickness and pressure of the gas volume has to be optimized for the wavelength range to be used. Many of the various scattering techniques that are presented in the following can be used also in combination with polarization analysis.

2.4 Neutron Detection

Efficient neutron detection is as important as the production of a high flux and efficient transport to the sample. The goal here is to convert close to 100% of those neutrons that reach the detector into counts. In addition as much of the available solid angle around the sample should be covered with detectors. In order to be able to extract physical information from the detected neutrons the detector must yield information on the position of the detection event as well as on the time. The latter is needed for all time-of-flight based methods, which are particularly important at pulsed (spallation) sources.

The kinetic energy of a thermal neutron is not sufficient to create a detectable signal in a counting tube or scintillator. Therefore detectors for neutron scattering rely on the energy release of a nuclear reaction, namely the absorption of the neutron. A suitable detector material must have a large absorption and the energy release should be such that it causes large ionization in a counting gas or intense light output in a scintillator. Only a few isotopes, listed in table 2.4, proved suitable for this purpose.

The use of a single detector that scans the scattering angle range step by step is a quite inefficient collection method and is replaced by the use of multichannel detectors that cover a whole range at once. The techniques used for this purpose range from assemblies of many single counting tubes, integrated counting wires in a sector covering gas detector (“banana”) to scintillation counters with position sensitivity. It was a long way from the first single BF_3 tube neutron counters of the early diffractometers and 3-axis spectrometers to modern large area position sensitive detector arrays. This development was fostered by the huge progress electronics, data acquisition and handling made in-between. The GBytes from square meters of position-sensitive and time resolved detectors are just becoming treatable. The use of ^{3}He as detection gas that serves as neutron converter and counting gas with low γ-sensitivity also was a big progress. Due to a severe shortage of ^{3}He which recently became obvious, now new concepts for efficient neutron detection are being investigated and developed in order to preserve the performance of neutron scattering instrumentation. Besides gas counters scintillation detectors with ^{6}Li as neutron converter in scintillating glass or mixed with ZnS as scintillator are used. Either they are combined with photomultiplier arrays or CCD cameras. The latter without single event counting and time resolution.

Image plates containing a neutron converter (Li or Gd) store the energy from neutron absorption events in a phosphor which after exposure (similar to a photographic film) is read-out by stimulating light emission from the phosphor with a laser and detection of the emitted light.

Isotope	$\sigma_a/10^{-24}\mathrm{cm}^2$	reaction	energy release /MeV
^{3}He	5333	$\mathrm{n} +^3 \mathrm{He} \rightarrow \mathrm{p} + \mathrm{t}$	0.76
^{6}Li	940	$\mathrm{n} +^6 \mathrm{Li} \rightarrow \alpha + \mathrm{t}$	4.8
^{10}B	3837	$\mathrm{n} +^{10} \mathrm{B} \rightarrow \alpha +^7 \mathrm{Li}^*$	2.3
^{155}Gd	60900	$\mathrm{n} +^{155} \mathrm{Gd} \rightarrow^{156} \mathrm{Gd} + \gamma\mathrm{s}$	conversion e $\simeq$ 60 KeV [11]
^{157}Gd	254000	$\mathrm{n} +^{157} \mathrm{Gd} \rightarrow^{158} \mathrm{Gd} + \gamma\mathrm{s}$	"
^{235}U	680	fission	170

Table 1: *Reactions that are used to detect thermal neutrons. Absorption cross sections are given for neutrons with v=2200m/s.*

3 Diffractometers

Neutrons are especially useful if hydrogen or other light element positions or magnetic structures are to be determined. Combination with X-ray diffraction then enables the separate visualization of atomic position and electron density maps.

3.1 2-axis diffractometer, powder diffractometer

In its essence the generic 2-axis type neutron diffractometer consists of a collimator that defines the beam direction and a (mosaic) crystal oriented such that Bragg reflection for neutrons of desired selected wavelength occurs into the collimated direction. The monochromatized neutrons then hit the sample and are scattered in different directions. A crystalline powder sample would produce intensity on Debye-Scherrer rings. The early simple neutron diffratometers used a single detector e.g. a BF_3 counting tube that scan the scattering angle, around the sample. Count rate detection as a function of scattering angle 2θ yields the diffraction pattern. Modern instruments [12, 13, 14] rather have position sensitive detector (arrays) that cover a large range of solid angle and different scattering angles. The corresponding lattice plane distance follows from

$$d = \frac{\lambda}{2\,\sin\theta} \tag{4}$$

The resolution is given by

$$\frac{\Delta d}{d} = \sqrt{\left(\frac{\Delta\lambda}{\lambda}\right)^2 + \left(\frac{\Delta\theta}{\tan\theta}\right)^2} \tag{5}$$

High resolution requires a well defined incoming wavelength and a well known scattering angle –except close to $2\theta = \pi$ –. In general one may scan the d-value also by changing the wavelength λ instead of scanning the scattering angle 2θ. At a pulsed source the λ tagging is given by the difference between start time of the pulse and neutron arrival time at the detector, $\lambda(\Delta t) = \Delta t\, h/(m_n\, L)$. h is the Planck constant, m_n the neutron mass and L the distance from pulse source and detector. Combination of an (area) detector array and the time-of-flight method yields a high detection data rate and is commonly used at pulse spallation sources [14, 15]. Even at a continuous reactor source the loss associated with a pulse chopper may pay-off [16]. At a short pulse spallation source very high resolution can be achieved by using a long flight path ($\simeq$100m) to tag the wavelength and concentrating detectors in the back scattering region,

i.e. $1/\tan\theta \to 0$. Examples for diffraction results obtained at the instrument POWGEN at the SNS is shown in figure 4.

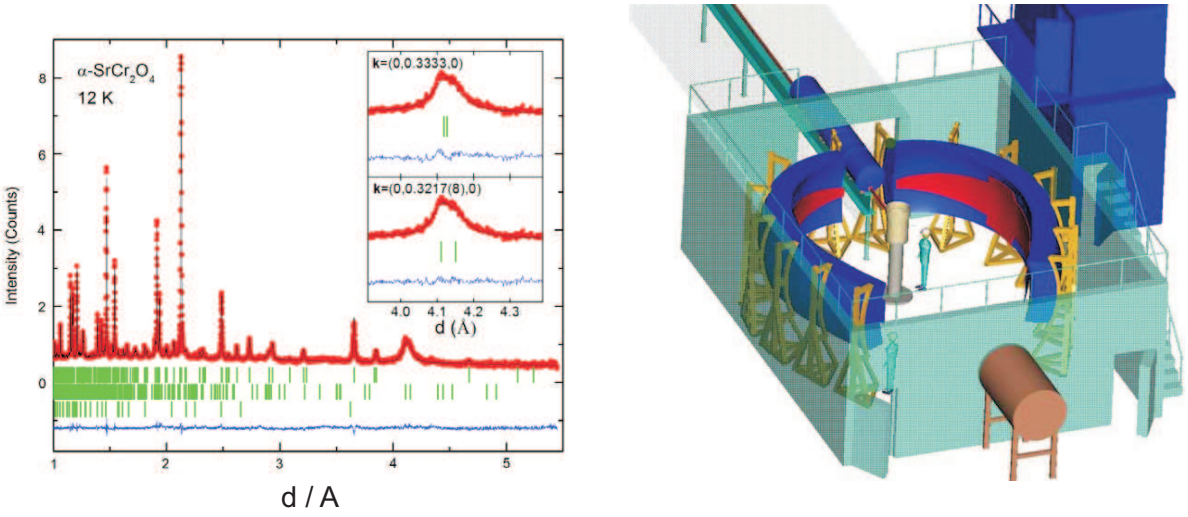

Fig. 4: *Example for a powder diffraction pattern as obtained at then time-of-flight diffractometer POWGEN at the SNS in Oak Ridge. The low temperature pattern here exhibits occurrence of magnetic reflections of an incommensurate helical structure around* $\mathrm{d} = 4.1\,\text{Å}$ *that are absent above the magnetic ordering temperature of 43 K. Precise determination of the lattice constants and correlating with the magnetic features indicate the presence of a magneto-structural coupling. [17] At the right side a sketch of the instrument is shown. The white neutron beam starts in the moderator at 60 m distance from the sample, it arrives through a neutron guide at the sample located in the center of the detector arrangement. The curved surface indicates the detector area, which is pixelated into about 240000 cells. Software correlates arrival time and pixel position and is used to accumulated data from a larger detector surface. The final result is seen in the diffractogram at the top.* **Figure (left part) from ref. [17] with permission, copyright IOP.**

3.2 Single crystal diffractometer

Single crystal diffractometers are used to measure the intensity of as many Bragg reflections in reciprocal space as possible in order to determine the structure of the unit cell. For crystals with small unit cells Bragg reflection intensity is only detected if both the scattering angle between incoming and detected neutron beam has the right value and in addition the crystal orientation must be such that the corresponding lattice planes fulfill the reflection condition. Therefore these spectrometers need a goniometer for sample orientation in addition to the ability to set the scattering angle.

Giving the sample orientation and the positioning of an arc of detectors more freedom to rotate around tilted axis and go out of the horizontal plane makes it possible to map the intensity of a selected plane in reciprocal space. This so-called *flat-cone* instrument [18] in particular also enables easy access to scattering intensity in-between the Bragg reflections in a reciprocal lattice plane (u,v) as e.g. $(h \neq 0, u, v)$.

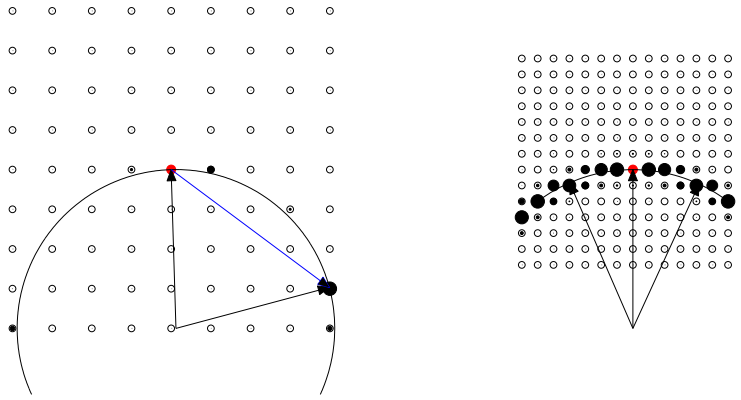

Fig. 5: *Ewald spheres in a reciprocal lattice from a small unit cell and from a large unit cell crystal (e.g. protein).*

In the case of very large unit cells as for protein crystals the curvature of the Ewald sphere is low enough that many reflections fulfill the Bragg condition within the resolution width simultaneously. Here a position sensitive detection with a sub-mm resolution is needed for an efficient data collection. At a continuous source the detector can either be an image plate or a scintillator screen with CCD camera. Wound into a cylinder with the sample position in the center an image plate detector can cover a very large solid angle at once. In this geometry it is possible to read-out the image plate in place. With CCD or other planar detectors a comparable solid angle coverage requires the use of many modules that are positioned around the sample. Figure 6 show a drawing of the BIODIFF experiment at the FRMII in Garching that utilizes this detection method, a sample diffraction image is also shown.
The sample crystal is then rotated around one axis and data are taken for each rotation step. Eventually the sample crystal has to be remounted in another orientation to complete the data collection. Reflections then are automatically indexed by software. A protein crystal analysis requires the collection of several 10000 individual reflex intensities. Only the use of area detectors like image plate CCD or other high resolution detectors makes this type of data collection possible in periods of a few weeks [19].
At spallation or other pulsed sources neutrons from an extended range of the continuous spectrum are to be used ("Laue method"). Unlike for the "Laue" at a continuous source overlap of reflection and λ-tagging can be done by the neutron arrival time. This rules out image plate and CCD-detectors, which have no appropriate time resolution. For those instruments only highly sophisticated and rather expensive high resolution gas detectors or position resolving scintillation detectors are suitable [20, 21].

4 Small angle scattering diffractometer and Reflectometers

Small angle scattering is a diffraction method for the observation of mesoscopic structures in the range between 1 nm and several 100 nm. In particular the possibility to vary the scattering contrast by exchange of H with D makes it a unique tool for soft-matter investigations (polymers, bio-molecular systems, complex fluids, gels etc.) [22, 23]. For the spatial resolution of

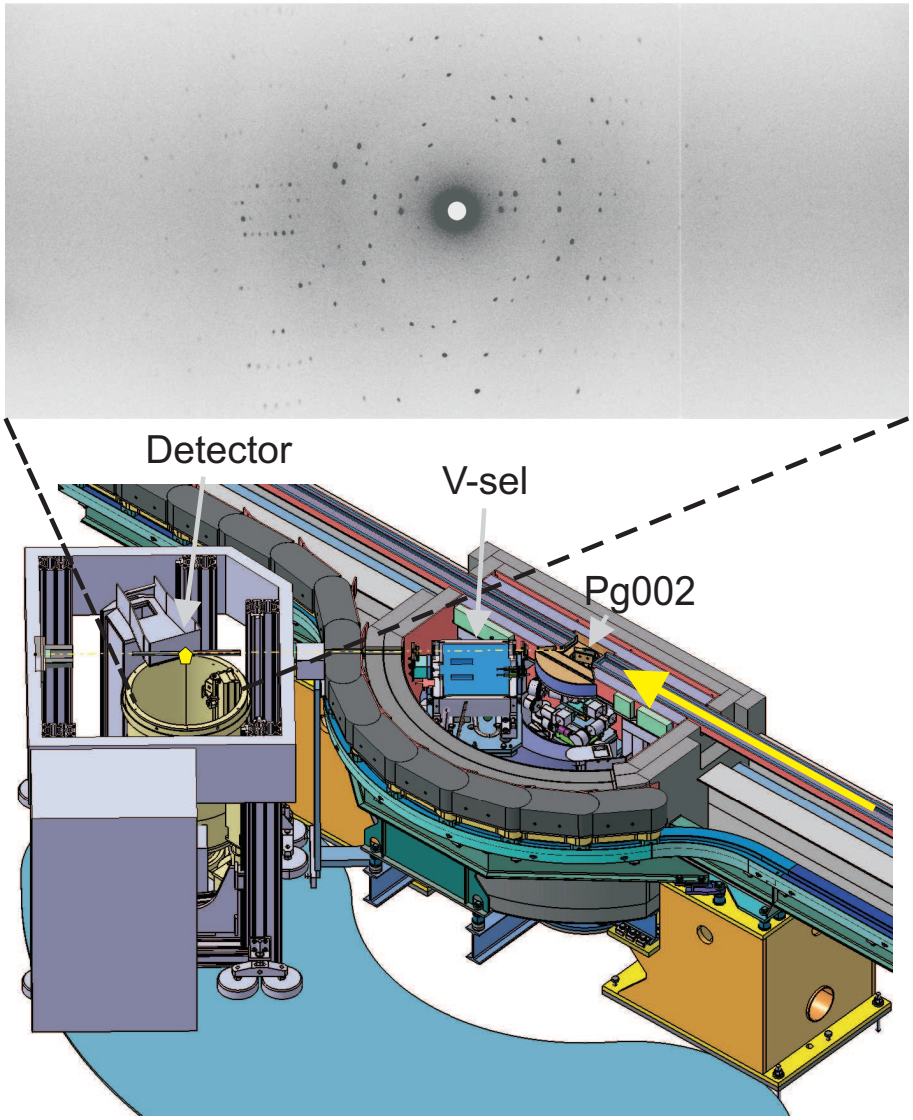

Fig. 6: *Reflections from a myoglobin crystal on the cylindrical image-plate of the BIODIFF macromolecular single crystal diffractometer at the FRMII in Garching. A considerable number of Bragg spots are seen for one sample orientation. A complete experiment comprises the data collection for many sample rotation angles and orientations in order to measure several 10000 intensities. The lower part of the figure displays a cut through the instrument. Neutron in the guide (indicated by the yellow arrow) are monochromatized and reflected by a graphite crystal, PG002. Higher order wavelength contaminations are removed by a velocity selector, v-sel. The narrow beam of a few mm diameter then leaves the lead shielding and enters the detector rack. The yellow polygon indicates the sample crystal. In operation the cylindrical image plate detector is raised such that the sample is in its center. The configuration shown is for exposure of the auxiliary CCD camera.*

SANS the sample can be described by a scattering length density $\rho(\mathbf{r})$ or better by the contrast $\Delta\rho(\mathbf{r}) - \rho_0$. The scattering length density results form assigning the sum of all nuclear scattering lengths, b_l within a molecular building block to the volume occupied by this block. ρ_0 is that of an embedding medium, e.g. a solvent. The the differential scattering cross section reads:

$$\frac{d\sigma}{d\Omega}(\mathbf{Q}) = \sum_{l,j}^{N} b_l b_j e^{-i\mathbf{Q}(\mathbf{r}_l - \mathbf{r}_j)} \quad \simeq \quad \left| \int \Delta\rho(\mathbf{r}) e^{-\mathbf{Q}\cdot\mathbf{r}} d^3\mathbf{r} \right|^2 \tag{6}$$

For colloidal objects in dilute concentration, as in the example in figure 8, the integral in eq. 6 can be done for one the colloidal particle objects multiplied by their number. For higher concentrations interference between objects modifies the cross section.

The principle of a *classical pin-hole camera* type small angle neutron scattering (SANS) instrument is rather simple. In its essence the proper camera consist of two pin-holes (entrance aperture and exit aperture) at a distance of several meters. The apertures have typical sizes of 3cm and 1cm and serve as collimator to define the direction of the incident neutrons. After hitting the sample closely behind the exit aperture, the scattered neutrons are detected by a position sensitive detector in a distance of 1 m up to several 10 m from the sample. The effective distance between the pin-holes and between sample and detector are variable in order to cover a broader Q-range. The basic setup is show in figure 7. Since neutrons are significantly scattered by air, it is necessary to evacuate the long flight spaces in the collimator and between sample and detector. Especially the latter implies that the appearance of a SANS instrument is dominated by a huge vacuum tank which contains the detector on rails to vary the distance for different Q-ranges and resolutions. The collimation length, i.e. the distance between exit and entrance aperture has to be chosen accordingly. This is done by introducing neutron guides into the space between velocity selector and current position of the entrance aperture. Thereby a beam with full divergence is lead until the effective start of the pin-hole collimation. The wavelength selection at a continuous source is performed with a typical relative width of 10% by the use of a mechanical velocity selector (see. 2.2). Typically a wavelength range between 5Å and 20Å is used for experiments. Example data from polystyrene spheres with different radii in dilute colloidal solution are shown in figure 8.

In principle a SANS experiment at a *pulsed source* looks quite similar to the one described above [24]. The main difference is that the velocity selector is omitted and replaced by the time-of-flight analysis of the neutrons arriving at the detector. The effective wavevector $\mathbf{Q}$ at a given detector pixel now depends on the arrival time of the neutron that tags its velocity. To arrive at the standard representation of SANS data in terms of $d\sigma/d\Omega(Q)$ grouping of pixels and time-bins yielding equal Q has to be performed by software.

To achieve instruments with *Ultra high resolution, USANS* one has to observe that the pin-hole collimation at the longest collimation distances yields a lowest $Q \simeq 10^{-3}\,\text{Å}^{-1}$. Since the size of both apertures enter this resolution limit and since the intensity is proportional to the product of both aperture areas, an increase of Q-resolution by this means is accompanied by a significant intensity reduction with the 4-th power of the resolution improvement. This effect poses a practical limit to the resolution. [2] Within a pin-hole instrument the use of neutron lenses can extend the Q-resolution. A focusing lens close to the sample position is used to

[2] A way out would be to make the instrument even longer. But the available space and the increasing costs set a limit. Note that the fact that the existing instruments are already very large are caused by this relation. Since the moderator is an extended source with a given brilliance intensity can only be gained by increasing the areas of source and sample. To keep the divergence in the limits posed by the resolution then requires large distances.

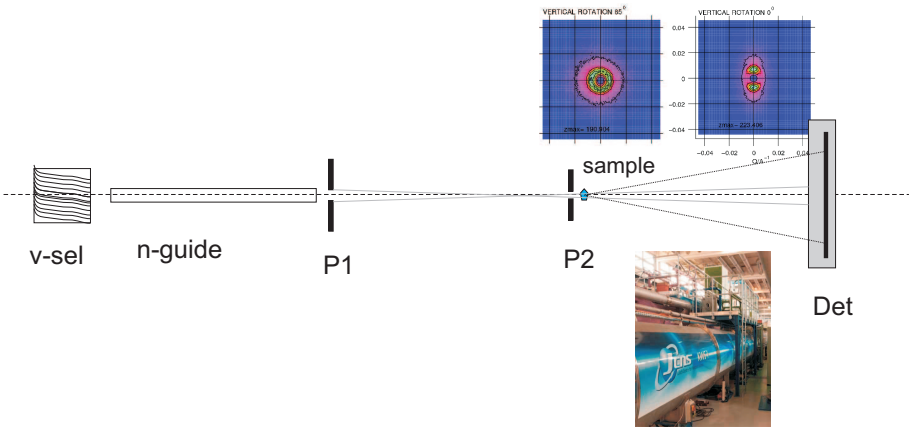

Fig. 7: *Schematics of a classical small angle neutron camera with pin-hole collimation. The collimation distance between the two pin-holes, $L_{\rm coll}$ is the same as the sample (at pin-hole P2) detector distance $L_{\rm det}$. After a velocity selector at the beginning a section with neutron guides bridges the distance to the first pin-hole. To vary the distance more or less neutron guide sections may be moved into the beam path. The detector can move in a vacuum tank to always match $L_{\rm det} = L_{\rm coll}$. Typical dimensions are $1 \cdots 40$ m for $L_{\rm coll}$ and 1cm for the sample pin-hole P1 and about 3cm for P2.*

produce an image of a small entrance aperture at the start of the collimation on the detector plane. The intensity loss due to the narrowing of the entrance aperture is mitigated by the larger aperture at the sample position which is only limited by either the lens diameter (some cm) or the available sample area or the divergence of the illumination of the input pin-hole. A neutron lens can be made from materials with low neutron absorption and large scattering length density $b\,N$. The small angle scattering of the used material and its surfaces must be very low. Single crystals of MgF are a viable choice. The refractive index $n = 1 - \lambda^2\, b\, N/(2\pi)$ is slightly smaller than 1. To get a reasonable focusing effect a larger number of biconvex lenses have to be stacked. In order to reduce intensity losses due to thermal diffuse scattering the lenses should be cooled [25]. By this means the lowest available Q can be extended by one order of magnitude. Limitations occur due to chromatic errors (i.e. the wavelength dependence of the refractive index and gravitation). In a *Focusing mirror SANS*, as illustrated in figure 9, chromatic errors can be avoided by using elliptical mirrors instead of lenses. The challenge here is the necessary quality of the surface such that its parasitic scattering stays orders of magnitude below the scattering intensity expected from a sample. [26] Other techniques as the *Double Crystal Diffractometer, DKD* or the *Spin Echo Small Angle Scattering, SESANS* even enable the exploration of scattering at very low angles that lead to real space dimensions in the μm range, which overlap with light scattering resolution. Due to the limited space we mention them only briefly here. First there is the double crystal method (DKD) which utilizes the reflection sequence from two perfect (silicon) crystals, which only happens when these are rotated to the same angle within μ rad. Minute deviations of neutron paths due to scattering lead to deviations of the rotation angle that transmits these neutrons. To obtain a diffraction pattern the crystal angle has to be scanned stepwise [27]. Wide range SANS data from a hierarchically structured sample obtained by a combination of pin-hole, focusing mirror and DKD SANS, are show in figure 10. Polymer containing wax crystallites arrange to larger aggregates that finally are even visible in a light microscope. Length scales from several micrometers down to the nm

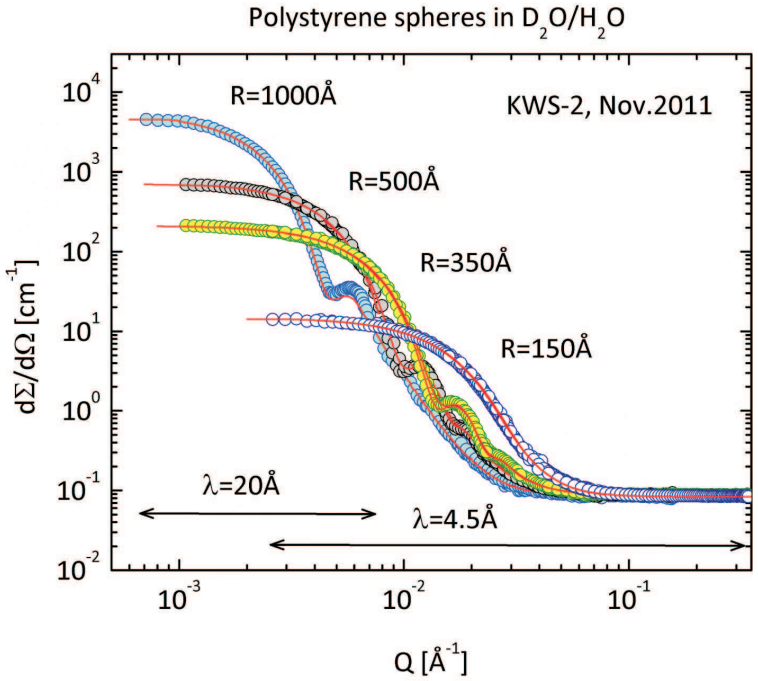

Fig. 8: *Reference examples of radially averaged SANS patterns from colloidal suspensions of polystyrene spheres of different sizes exploring the range of the typical pin-hole SANS-camera, here KWS-2 at the FRMII using different wavelength and collimation lengths.*

thick wax platelet size are covered. A different high resolution method utilizes the coding of small angular deviations in spin precession of the neutron (SESANS) [28]. As Fourier method it may be imagined similar to the projection of a more or less narrow sine stripe pattern on an integrating detector with a matched stripe mask. If small angle scattering distributes neutron such that their deviation is large enough to go from a maximum of a stripe to the adjacent minimum, the contrast (variation) upon shift of the stripe mask is reduced or vanished.

The specular reflection from a planar surface contains information on the scattering length density profile perpendicular to the surface, which is made accessible by *neutron reflectometers*. Beyond the total reflection, which depends on the scattering length density of the substrate, the Fresnel reflectivity $\propto Q^{-4}$ is modulated according to the Fourier transform of the density profile across the surface. Lateral structures in addition give rise to off-specular scattering (see also 4). In order to measure the specular intensity a good angular resolution is needed only in the direction perpendicular to the surface whereas in the parallel direction a large divergence can be accepted. This illumination condition is realized by a slit collimation, focusing (by e.g. elliptical mirrors) in the direction along the slit may be used to get more neutrons on a small sample area. The intensity, i.e. the reflectivity, varies over many decades from 1 below the total reflection edge dropping with the general decay of Fresnel reflectivity $\propto Q^{-4}$ into the background level in the order of 10^{-6}. Variation of Q is either performed by a variation of the inclination angle or –using a fixed angle– by variation of the wavelength. At a pulsed source the latter method with time-of-flight analysis of the wavelength is the natural choice. Even at reactor sources the time-of-fligth method is used in some cases since it leaves the geometry fixed

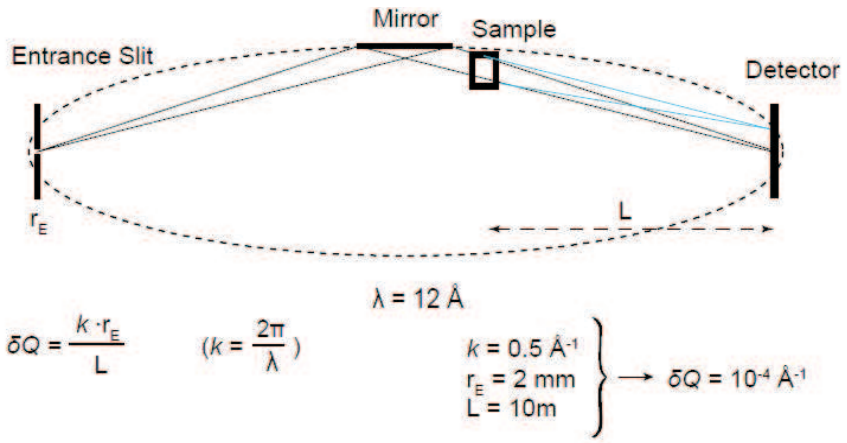

Fig. 9: *Principle of a focusing small angle neutron scattering setup which yields very high resolution in terms of the lowest observable wavevector. The focusing element is a mirror that maps a small pin-hole at the entrance of the spectrometer to a small spot on the detector. Thus very small angular deviations in the order of spot-size/sample-detector distance can be resolved. The intensity loss due to reducing the entrance pin-hole area is (partly) compensated by the large divergence that is accepted by the focusing element. The sample must be of the same area as the acceptance aperture of the focusing element, i.e. intensity is regained by illuminating a larger amount of sample.*

and there are no deformations of the reflectivity curve due to variation of the illuminated area, which occur when the sample is rotated. A recent instrument of this kind is e.g. the BioRef reflectometer at the HZB [30]. The most versatile detector at such an instrument is an area detector that allows for simultaneous measurement and immediate separation of specular and off-specular intensity. The off-specular scattering that can be analyzed in this configuration is located around the specular reflection a differing take-off angles. Since the typical reflection angles are small the structures that determine this off specular scattering are seen by the neutron beam in a projection with large contraction. Therefore in real space the corresponding scattering length density modulation are in the micrometer regime. In the perpendicular direction the off-specular scattering is sensitive to length scales that match those of a normal SANS experiment. If these modulations are also to be observed the wide divergence in the direction parallel to the surface cannot be used. Thus this special feature of a reflectometer cannot be used and therefore the experiment matches the abilities of a normal SANS instrument with *grazing incidence of the beam, GISANS*. Figure 11 shows a sketch of the scattering geometry together with example data from a microemulsion structure close to solid surface. The only difference is that now the sample is a planar surface which has to be positioned at the sample position such that the angle of incidence of the incoming neutron beam is the desired angle of specular reflection. To scan this the inclination angle of the sample must be scanned. The pattern with specular and both types of off-specular intensity is registered by the SANS area detector. The main difference to a standard SANS experiment then is the way how the data are to be interpreted, which is more complex [31].

The investigation of *magnetic layers* often needs *polarization analysis and magnetic field* at the

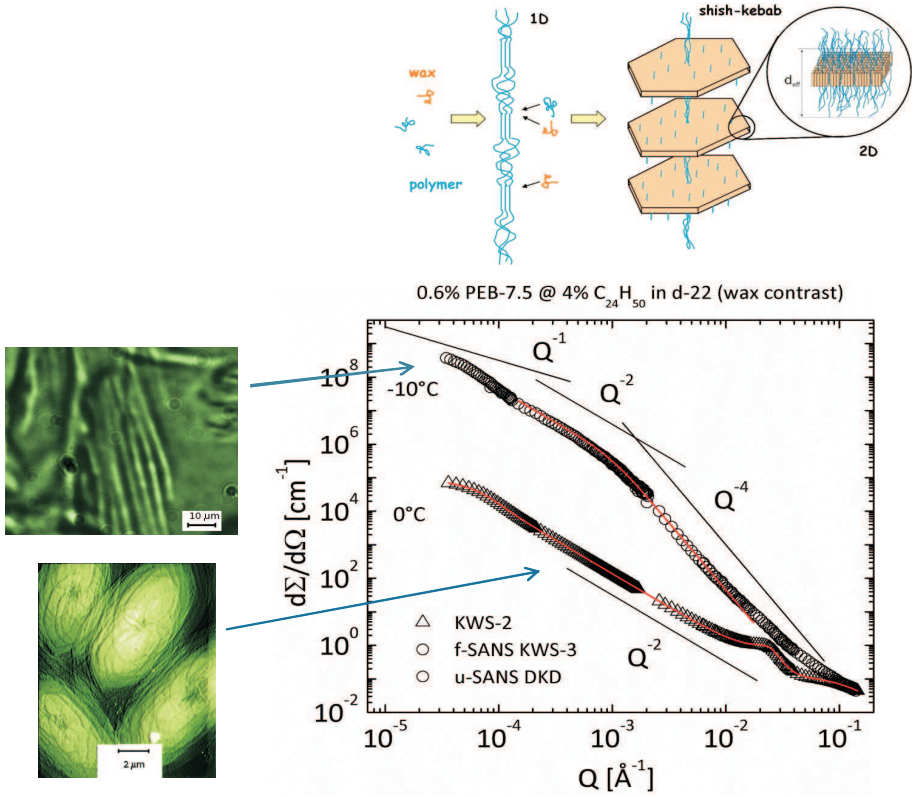

Fig. 10: *Application of a combination SANS techniques that span a very wide range in spatial resolution on a system with hierarchical structure formation. Here copolymers that are able to influence the crystallization of wax in alkanes (Diesel fuel) upon cooling are investigated in action [29]. Figure: courtesy Aurel Radulescu.*

sample. Thus there are 4 different reflectivities that can be measured by the possible combinations of incident polarization (up, down) and detected polarization (up,down). Polarization of the incident beam can be achieved using a magnetic multilayer, analysis of the reflected beam may also benefit from ^{3}He analyzer (in particular if GISANS is required). The up-down switching is performed by π-flippers which e.g. consist of a rectangular coil of Al-wire such that the neutron that enter the flipper suddenly "see" a different field orientation. The field is tuned such that a 180^0 rotation of the neutron spin is performed during its passage.
In *soft-matter and biology* an important application of neutron reflectometry pertains the structure of *liquid surfaces* covered e.g. by surfactants or similar molecules. The air liquid interface here is necessarily horizontal and cannot be tilted during scans. Thus a suitable reflectometer must supply a tilted incoming beam direction. Modern reflectometers of this type are e.g. the Platypus reflectometer at the OPAL reactor [32], the FIGARO reflectometer at ILL or at pulsed spallation sources the Liquids reflectometers at the SNS [33] and JPARC [34].

5 Spectrometers

Investigation of motions and excitation requires the analysis of energy transfer during scattering. Besides a defined and known energy before the scattering also the measurement of the neutron

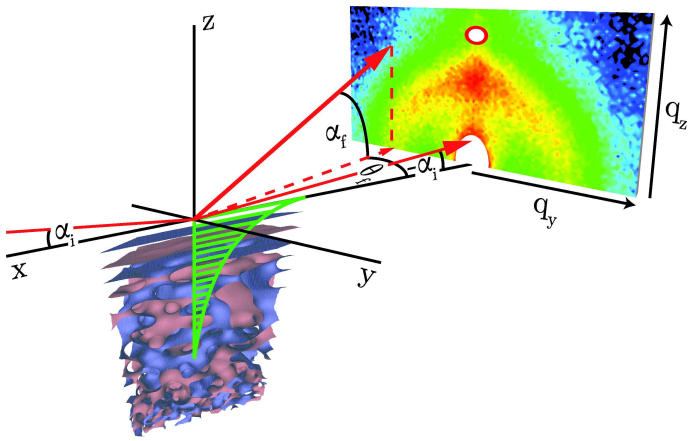

Fig. 11: *Grazing Incidence Small Angle Neutron Scattering (GISANS) geometry as it may be realized with a pin-hole SANS camera. The sketch shows –as example– a microscopic sample structure of bicontinuous microemulsion that becomes lamellar close to the surface [31]. The neutron beam enters through the material of the confining surface (e.g. Si or sapphire) at an angle below the total reflection limit. Thus the neutron enter only a small interface layer of the microemulsion in form of an evanescent wave. The penetration depth depends on the incident angle α_i and the wavelength. Figure: courtesy Henrich Frielinghaus*

energy after the scattering, i.e. in course of the detection is required. Depending on various combinations of energy ($\hbar\omega$) and momentum transfer (Q) resolution different types of neutron spectrometers are available.

5.1 Three axis spectrometer

The most obvious type of a neutron spectrometer emerges from a 2-axis diffractometer by adding a crystal Bragg reflection in the path between sample and detector. The additional rotation axis of the analyzing crystal gives this type of instrument its name: 3-axis spectrometer. The incoming wavelength is determined by the refection angle at and type of the monochromator crystal (axis 1), the incident direction is then defined using a Soller-type collimator, then the incident beam hits the sample and the scattered neutrons in a selected direction as set by the angle of the scattering arm (axis 2) and a collimator carried by it is analyzed. The analysis pertains its wavelength distribution which is determined by Bragg reflection at an analyzer crystal, the angle (axis 3) that determines the reflected wavelength. After the analyzer crystal the neutrons are counted by a detector. Eventually another collimator is used between analyzer crystal and detector. The angles may be scanned in different combinations to realize a desired path in reciprocal space $(\mathbf{Q}, \omega)$. E.g. scans at a given constant energy transfer $\hbar\omega$ may be performed along a line in $\mathbf{Q}$-space or ω may be scanned at constant $\mathbf{Q}$. In addition this may be achieved using a constant incident wavevector k_i or a constant final k_f wavenumber or some combination. If the sample is not isotropic but a crystal with excitations (e.g. phonons) that depend on $\mathbf{Q}$ a scan typically also implies rotation of the sample table respectively 3D reorientation of the sample. The instrument typically has a resolution in the order of (a few) percent. It is very versatile in the ability to set the focus to an arbitrary point in $\mathbf{Q}, \omega$ space. However, only one point at a time can be measured leading to a low data collection rate. Modern realizations of 3-axis (and similar) neutron instruments have a flexible mechanics that relies on elements as sample carrier,

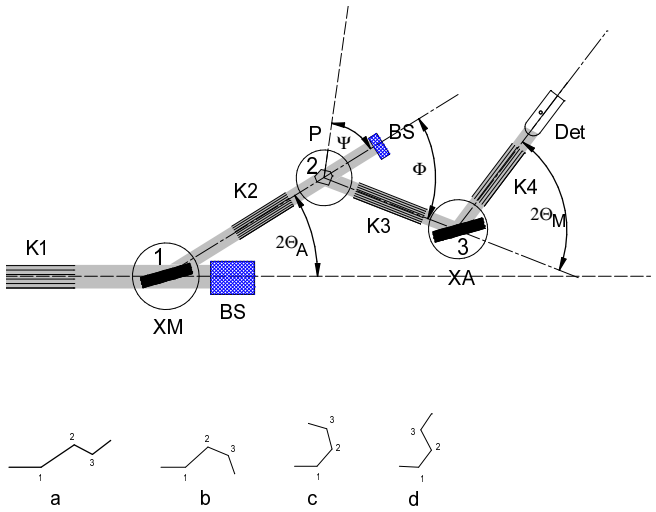

Fig. 12: *Schematics of a 3-axis spectrometer. Divergence is controlled by the collimators K1···4, the incident beam is monochromatized by a crystal XM (axis 1), the detected neutron wavelength is selected by the analyzer crystal XA (axis3). The sample is located at axis 2. Around this axis the scattering angle Φ is varied as well as the sample rotation Ψ. BS denote a beam stop. Patterns a-d show variants of spectrometer settings that can be used to sample the same $\mathbf{Q}, \hbar\omega$ point, however, the shape of the resolution is different. The latter fact is e.g. used to align an elongated tilted resolution ellipsoid to the slope of a dispersion surface.*

analyzer, analyzer detector etc. on air cushions that glide at $20\mu\mathrm{m}$ height on a marble or granite floor (Tanzboden). They are connected by levers that allow determination of the relative angles using resolvers. This enables a precise positioning of these several 100kg heavy modules. To improve the neutronic performance focusing monochromators and analyzer or analyzers that consist of crystal arrays, which reflect neutrons to an array of detectors, are employed [35]. Polarization analysis is achieved by using Heusler alloy crystals as monochromator and analyzer. For cold neutrons also magnetic supermirros and for large divergence ^{3}He cells are also in use. Three axis spectrometers are especially suited to measure excitations like phonons or magnons in single crystalline samples and to map their dispersion. An example for the measurement of magnon dispersion in copper pyrazine(pz) perchlorate measured at the PANDA 3-axis spectrometer [36] is shown in figure 13.

5.2 Time-of-flight spectrometers

Even at continuous sources time-of-flight spectrometers that utilize the stream of incoming neutrons only during about 1% of the time are well established work horse instruments. They use the flight time of neutrons over a defined path to yield information on their velocity and thus their wavelength and energy. The 3 basic different variants are the following.

- Generic time-of-flight (TOF) instrument (left part of figure 14): monochromatized beam from a crystal monochromator, chopper to create pulses (neutron bunches) in front of the sample, flight path of a few meters to detectors positioned around the sample. The final energy is inferred from the time delay between chopper opening and arrival of the scattered neutrons at the detector.

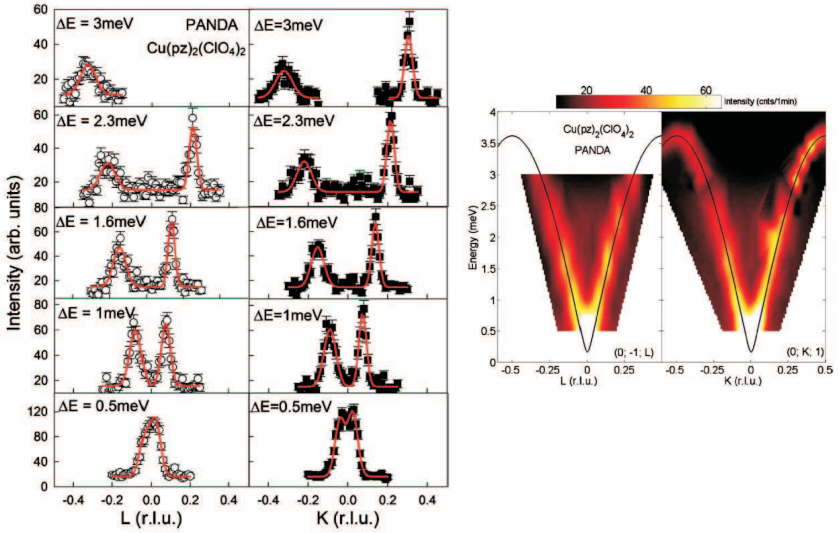

Fig. 13: *Dispersion of a gaped spin excitation at the antiferromagnetic zone center in the 2D-lattice antiferromagnet* $\mathrm{Cu(pz)_2(ClO_4)_2}$ *at low temperature (T=1.42 K) and zero external magnetic field. The left side shows two series of constant energy,* ΔE*, scans along the* $[0, k, 1]$ *and the* $[0, -1, l]$ *lines in reciprocal space. The right side compares the thus mapped excitation intensities with computed dispersion curves from linear spin-wave theory with next- and next-next- neighbor interactions. Figures from [36] with permission, copyright APS.*

- TOF-TOF instrument: instead of a crystal monochromator the incident beam path contains several choppers at a distance such that the time difference between chopper openings determines the incident neutron speed. The last chopper in front of the sample creates the neutron bunches and the detection is analog to the generic TOF.

- Inverted TOF instrument (right part of figure 14): starting from a pulsed source (chopper or spallation source) a "white" neutron beam is carried over an analyzing distance to the sample. After the sample the scattered neutrons are analyzed using an array of crystals before they reach the detectors. The final energy is fixed and determined by the analyzer crystals, the initial energy depends on arrival time of the neutrons.

The loss of intensity that is implied by the chopping of a continuous beam is largely overcompensated by the use of a large detector area that covers a very large solid angle $\Delta\Omega$ and by the fact that the whole spectrum of arrival times is collected quasi simultaneously.

State-of-the-art TOF spectrometers are equipped with position sensitive detectors that cover a huge solid angle. E.g. the IN5 spectrometer at the ILL [37] with a flight path of 4m has a detector coverage of $10\,\mathrm{m}^2$ in 100000 pixels. The energy resolution of TOF instruments is one of its defining properties, it depends on the variations of the neutron flight paths ΔL and variations in the time determination Δt. ΔL depends on the size and geometry of the sample and the variation of the exact neutron interaction location in the detectors. Both variations are in the range of several mm to cm. The time determination mainly depends on the chopper opening time, respectively the source pulse length (several 10 to 100μs). In addition the degree of monochromatization of the incoming (or in case of the inverse geometry outgoing) neutrons,

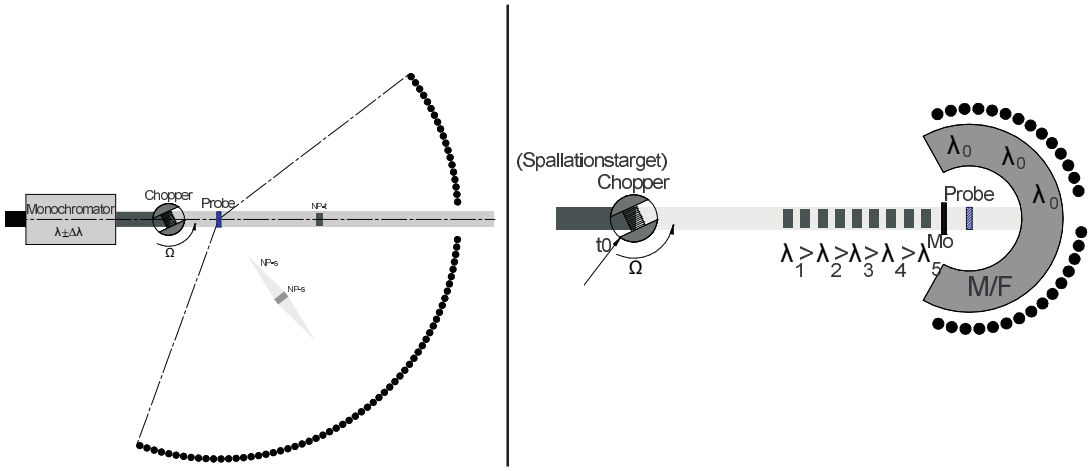

Fig. 14: *Schematics of neutron time-of-flight (TOF) spectrometers. Left: the normal geometry variant, which utilizes a monochromatizes incoming beam. A chopper in front of the sample creates a chain of short neutron bunches of uniform velocity. If the scattering is elastic neutrons from a bunch arrive at the same time at one of the detectors around the sample. Inelastically scattered neutrons vary in velocity and arrive earlier or later at the detector depending on the size and sign of the energy transfer $\hbar\omega$ during scattering. Right: inverted geometry spectrometer. Here the time-of-flight analysis of neutron energy is performed in a flight path before the sample, e.g. between sample and moderator of a pulsed source. After the sample only neutrons of a defined energy are transmitted to the detectors. The final analysis typically requires some kind of crystal Bragg reflection.*

$\Delta\lambda$ enters into the resolution width $\Delta\omega$:

$$\Delta\omega \;=\; \sqrt{(\frac{m_n L}{\hbar t^2}\Delta L)^2 + (\frac{m_n L}{\hbar t^3}\Delta t)^2 + (\frac{4\pi^2\hbar}{m_n\lambda^3}\Delta\lambda)^2} \tag{7}$$

Since $\lambda' \propto 1/v' \propto t$ close to the elastic line ($\lambda' \approx \lambda$) $\Delta\omega \propto 1/\lambda^3$. Thus the most efficient measure to increase the resolution is to increase the wavelength. This may be limited by the steep decrease of the source intensity towards long wavelength and/or by the restriction of momentum transfer range, since $Q_{\max} \propto \lambda^{-1}$. The relation for the inverse geometry TOF spectrometer are equivalent if λ is exchanged with λ'.
At larger energy transfers the nonlinear relation between time-of-flight and energy as well as the dependence of **Q** on the energy transfer becomes important (t_0, t = flight times of elastically scattered (or transmitted) neutrons and others, L flight path from sample to detector):

$$\omega(t) = \frac{m_n}{2\hbar}L^2\frac{t^2 - t_0^2}{t^2 t_0^2} \qquad\qquad Q = \frac{m_n}{\hbar}L\sqrt{\frac{t^2 + t_0^2 - 2cos(2\Theta)t_0 t}{t_0^2 t^2}} \tag{8}$$

For equal opening time of one histogramming channel the covered ω interval of one channel becomes strongly energy dependent, which has influence on the resolution at high energy transfers

and on the weighting factor connecting raw data with $S(Q,\omega)$

$$I(2\Theta,K) \propto \int_{(K-1)\Delta\tau}^{K\Delta\tau} \frac{k'}{k} 4\pi b^2 S(\mathbf{Q},\omega(t)) \frac{d\omega}{dt} dt \simeq 4\pi b^2 \frac{m_n}{\hbar} L^2 \frac{t_0}{t^4} S(\mathbf{Q}(t,2\Theta),\omega(t))\Delta\tau \qquad (9)$$

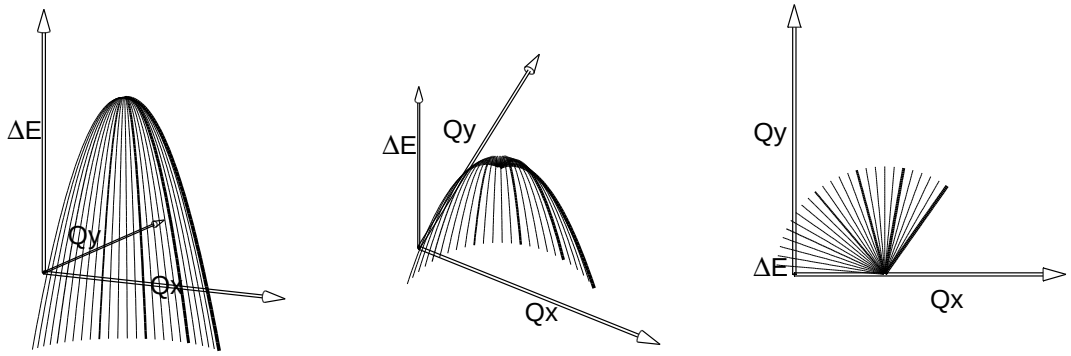

Fig. 15: *The volume in $(\mathbf{Q},\omega)$ space that is accessible in a time-of-flight neutron experiment. The indicated range corresponds to scattering angle between 5^0 and 130^0). Three different views are shown.*

The correlation between the energy and momentum transfer restricts the accessible volume in reciprocal space to the region indicated in figure 15.
The typical structure of TOF-data from a liquid is illustrated in figure 16 where the relations between arrival time an wavelength, energy transfer an Q is shown. The time-of-flight scale is proportional to the scattered, outgoing wavelength. The time corresponding to λ_0, the incoming wavelength (here $6\,\text{Å}$) is the position of the elastic scattering (typically the most prominent peak in the spectrum). Close to the elastic peak the momentum transfers Q of the curves for different angles are well separated and the quasi-elastic broadening of the spectra can be associated to the diffusive motion of the water molecules (tagged by the dominant incoherent scattering of the protons). Towards shorter times of flight the energy scale (dashed blue curve) and the Q scale becomes highly non-linear approaching infinity at t=0. The different spectra belong to different scattering angles. The cutoff of the inelastic spectra at short but finite time corresponds to the temperature of the sample, beyond the k_BT cutoff energy gain of the neutron becomes increasingly improbable. The energy gain part of the neutron on the other side is stretched to infinite time where the limit E_i is reached. The spectrum at that side becomes increasingly diluted in time and therefore featureless and very weak, such that a practical end has to be set. The thus established range determines the possible repetition frequency of the chopper. In contrast for a spectrometer with inverted geometry, gain and loss side are exchanged, such that excitations beyond the thermally occupied states can be excited by the neutron and detected in the spectrum. The quasi-elastic scattering around the elastic line position broadens with increasing Q and results from diffusion whereas the high energy part corresponds to vibration like motions in the liquid. The scattering intensity dominantly results from the incoherent scattering of the protons in the sample. Thus the measured spectra correspond to the self-correlation of proton motion.

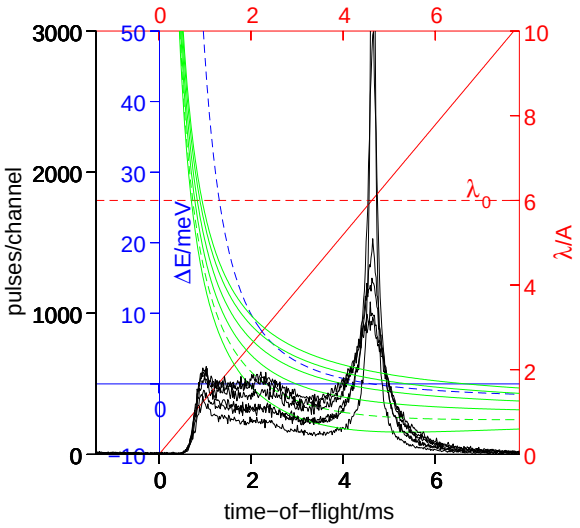

Fig. 16: *Raw time-of-flight spectra of liquid water at ambient temperature. The plot illustrates some general features of the type of information obtained.*

Another, modern example is shown in figure 17 where the position information from the detector of a disc chopper TOF spectrometer is used to directly map the magnon dispersion curve of the quasi one-dimensional antiferromagnet $(CH_3)_2CHNH_3CuCl_3$ [38].

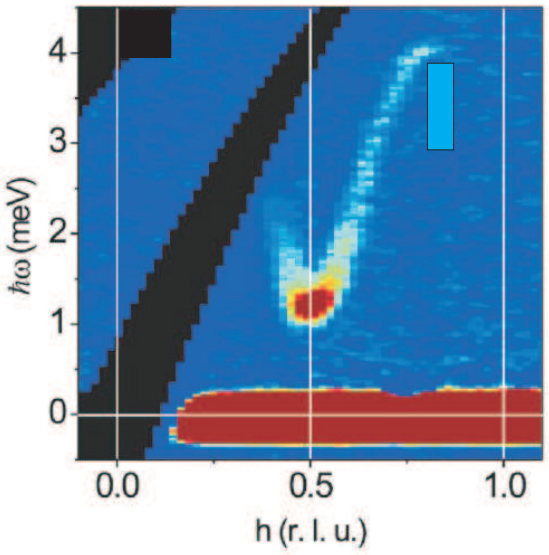

Fig. 17: *Magnon dispersion directly visible in the pixel resolved spectra from the DSC time-of-flight spectrometer at NIST, Gaithersburg [38] Figure from ref.[38], with permission, copyright APS.*

5.3 Backscattering for high resolution

To extend the energy resolution down to the μeV range energy/wavelength selection Bragg reflection from perfect crystals (e.g. the (311) reflection from Si wafers) at an angle 2Θ close to 180^0 is used. The resulting $\lambda = 2d\sin(\Theta \pm \delta\Theta)$ then only depends to second order on the divergence $\delta\Theta$. This allows to compensate the intensity loss due to the a narrow wavelength selection by allowing for a large beam divergence. At a continuous source the principle layout of a so called backscattering instrument is illustrated in figure 18. The variation of the energy transfer $\Delta E = \hbar\omega$ is achieved by the Doppler effect due to movement of the monochromator crystal in beam direction. After scattering at the sample the neutrons are analyzed by Bragg reflection backscattering from large area crystal covered "mirrors" (figure 19) that focus the intensity from a huge solid angle onto a detector. To stay in the backscattering condition theses detectors have to be close to the sample. Neutrons scattered by the sample that enter the detectors directly are discriminated from those that were analyzed by reflection at the crystal covered mirror by the longer time of flight they need for the return travel from sample position to the analyzers. At a continuous source that requires the use of a coarse chopper with about 50% opening. The chopper can be combined with mosaic crystals (PG002) that reflect neutrons from an initial white beam to the monochromator on the Doppler drive. The crystals move with the rotation of the chopper wheel and by that (if the rotation velocity is adapted) the correlation between angle and wavelength that results from the Bragg reflection condition from a mosaic crystal is modified such that the divergence of the beam is increased and at the same time the wavelength angle correlation is compensated. Then a large (focusing) monochromator crystal can be used and more intensity is available for scattering [39, 40].

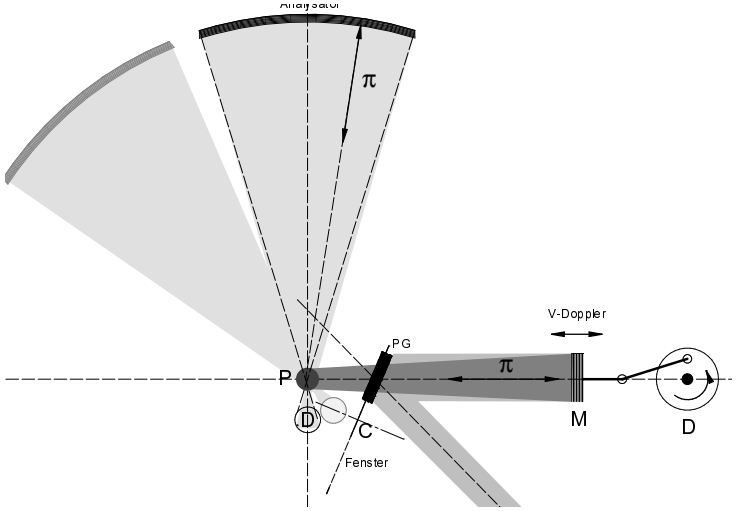

Fig. 18: *Schematics of the salient features of a backscattering spectrometer. The high resolution in the range of $\hbar\omega \simeq 1\ \mu$eV is achieved by nearly 180^0 reflection (backscattering) from perfect crystals in both the monochromator and the analyzer. The energy scan is performed by moving the monochromator in beam direction utilizing the Doppler effect to shift the neutron velocity. The intensity loss due to the narrow velocity filtering is compensated by the large solid angle covered by the analyzer segments. Each analyzer segments focuses the reflected neutrons onto one small detector.*

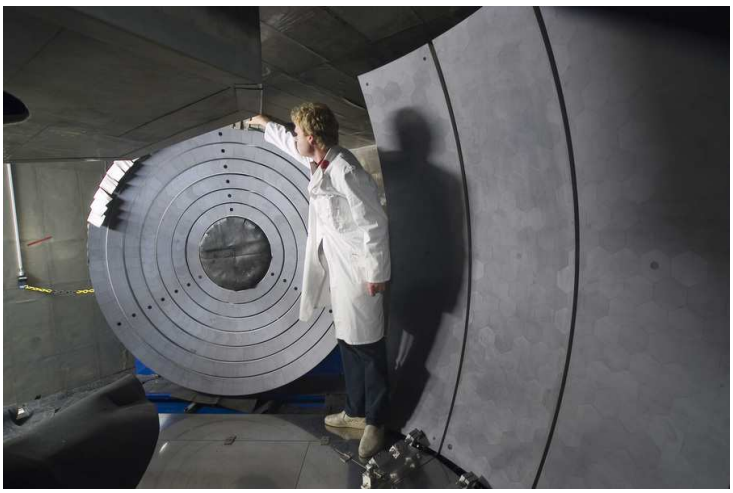

Fig. 19: *View towards the crystal covered analyzer mirrors inside the SPHERES backscattering spectrometer at the FRMII. Complete rings correspond to equal Q zones at small Q the large sectors cover the larger momentum transfers.*

As example the transition from quasi-elastic jump rotation to tunneling of CH_3 groups in theophylline with decreasing temperature is illustrated in figure 20. Due to limitations of the Doppler velocity and the finite bandwidth of the illumination via reflection from a PG002 crystal the energy width of the measured spectrum is restricted to $\pm 30 \mu\mathrm{eV}$. The energy resolution reaches values of $\Delta\hbar\omega \simeq 0.7\,\mu eV$.
This limitation is released if backscattering for analysis of scattered neutrons is used in an inverted geometry TOF instrument as e.g. the BASIS backscattering spectrometer at SNS [41]. Here the monochromatization of the beam is performed by TOF analysis with a path length of $\simeq 80\,\mathrm{m}$, the distance of the spectrometer from the moderator of the pulsed source. With these parameters BASIS achieves an energy resolution of $3 \cdots 4\,\mu\mathrm{eV}$ and a width of the spectrum of several 100 $\mu\mathrm{eV}$.

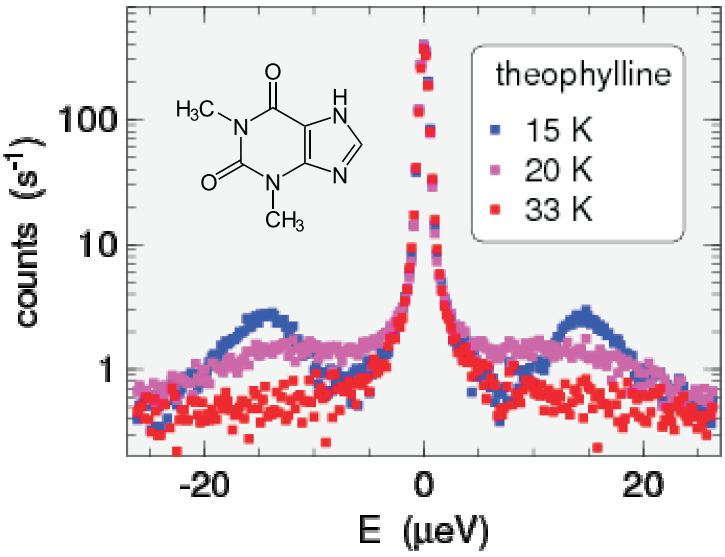

Fig. 20: *Backscattering spectrum showing tunneling lines of CH_3-groups in theophylline at low temperature and the transition to quasi-elastic rotational diffusion with increasing T.*

6 Neutron Spin-Echo Spectrometers

In general an improvement of the spectral resolution requires the narrowing of the filter transmission functions **before** (monochromator) and **after** (analyzer) the sample scattering by the desired resolution improvement factor. This implies an intensity reduction by the square of the resolution improvement factor. The attempt to increase the resolution of the TOF instruments far beyond the $\Delta E/E \approx 0.1 \cdots 1\%$ of the present realizations would lead to an unacceptable loss of intensity (as expressed in terms of detector count rate). However, it is possible to use the neutron spin directions as kind of individual stop watch pointers, thereby allowing the use of a broad velocity band (i.e. intensity) of the incoming neutron beam. The clockwork of this watch is then effected by the precession of the neutron spins in an external magnetic field [42]. [3] The restrictions affecting application are caused by the fact that the "spin-stop watch" can only be read up to an unknown integer number of complete precession turns. The scattering function $S(Q,\omega)$ is not such that there is only one defined velocity change induced but Δv is distributed according to $S(Q,\omega \approx k\Delta v)$. The detector signal is proportional to the integral of precession-angle-cosine modulated intensity contributions with weight according to $S(Q,\omega)$ corresponding to $\Delta\omega \propto \Delta v$. Therefore the signal of the NSE spectrometer is different from the TOF histograms of classical TOF-spectrometers. Instead it is proportional to the cosine-Fourier transform of $S(Q,\omega)$, i.e. the intermediate scattering function $S(Q,t)$.
A concrete setup of a NSE spectrometer is presented in the lower part of figure 21, the upper part shows the directions of the spin expectation value during the passage of a neutron through the spectrometer. Longitudinally polarized neutrons (i.e. spin expectation value parallel to the

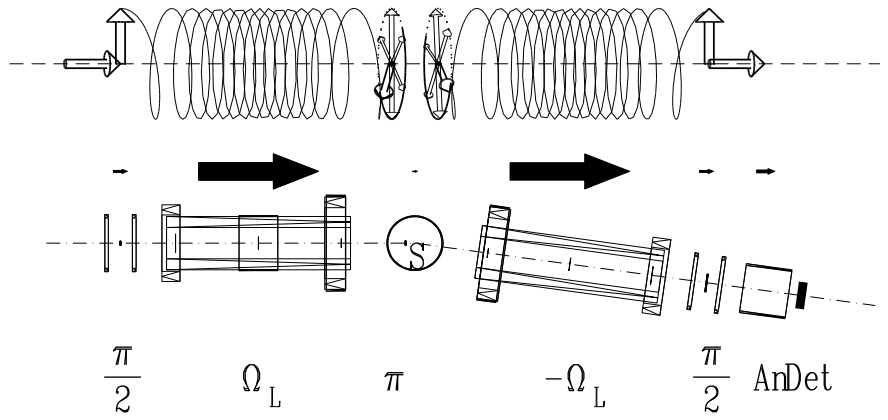

Fig. 21: *Spin rotations and setup of a generic NSE-spectrometer. Upper part: Spin rotation, middle part: magnitude of the magnetic field, lower part: schematic setup of the Jülich NSE-spectrometer.*

beam direction) enter the spectrometer from the left. In the first so-called $\pi/2$-flipper the spin is rotated such that on exit it is orthogonal to the longitudinal magnetic field of the precession

[3] It is somewhat involved to extract this analogy starting from a quantum mechanical view with spin eigenstates and eigenvalues. Implicitly we are talking about the behavior of the ensemble average of the spin vectors which obeys the "classical" Bloch equation concerning its precession in the magnetic field. As long as the kinetic energy of the neutrons is much bigger than the magnetic level splitting the classical picture is completely sufficient and much easier to visualize to understand the NSE spectrometer than a quantum mechanical treatment.

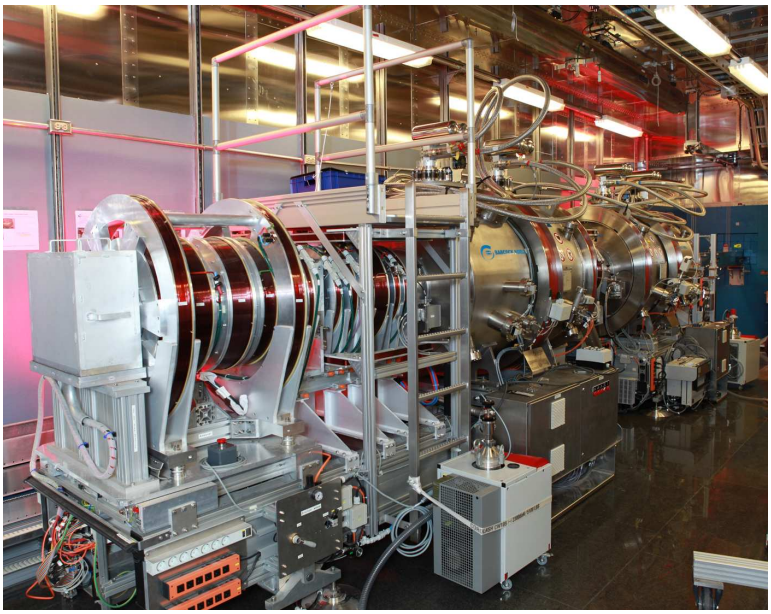

Fig. 22: *View to the NSE instrument at the SNS [43] seen from the detector end. From left (close) to the right (far) one can see the detector, the solenoids around the analyzer, the two cryostats for the superconducting main solenoids (the sample position is between these) and at the far end the blue surface of the shielding that contains the neutron guide system with frame overlap choppers. The target moderator position is 11m behind this wall.*

path. That defines the start of the "spin stop watch", immediately after the flipper a precession of the spins around the axial magnetic field begins. The precession frequency increases during the approach of the center of the main precession solenoid, where it reaches its maximum of up to a few MHz. The accumulation of precession angle continues –with decreasing frequency– until the neutrons reach the π-flipper close to the sample (S). The total precession angle at that point is:

$$\Psi_{1,2} \;=\; \frac{\gamma}{v}\underbrace{\int_{l_{1,2}} |B| dl}_{J_{1,2}} \;=\; n2\pi + \alpha \;=\; \frac{\gamma J_i}{v} \tag{10}$$

where $\gamma = 2\pi \times 2913.06598 \times 10^4 \mathrm{s}^{-1}/\mathrm{Tesla}$ is the gyromagnetic ratio of the neutrons and $|B|$ is the modulus of the magnetic induction along the primary or secondary path $l_{1,2}$.
Close to the sample (ideal: at the sample position) the so-called π-flipper is located, it rotates the spins by 180^0 around a vertical axis, thereby the total precession angle is transformed to $\Psi_1 = n2\pi + \alpha \rightarrow n2\pi - \alpha$. The parameters n and α are –according to eqn. 10 – extremely dependent on velocity and therefore very different for different neutrons in a beam with finite width of the wavelength distribution. As a consequence the spin vectors at the sample position (π-flipper) are evenly distributed on a disc orthogonal to the field direction. If no velocity change occurs during scattering at the sample (elastic scattering) each neutron enters the secondary arm of the spectrometer with unchanged velocity. The precession field and path length of the secondary arm exactly match the corresponding elements of the primary arm before the sample (π-flipper). Accordingly the precession accumulated in the secondary arm is $\Psi_2 = n2\pi + \alpha$ and the total precession angle at the second $\pi/2$-flippers is $\Psi_1 + \Psi_2 = (n+n)2\pi - \alpha + \alpha = 2n2\pi$.

I.e. all spins –irrespective of their initial velocity– reassemble at the same vertical position they had at the start point, the rotation imposed by the second π-flipper converts this back to the initial longitudinal polarization that is fully restored. The flippers limit the the two race tracks and realize "start", "time reversal" and "stop" of the "spin stop watches". The second $\pi/2$-flipper is the last element used to manipulate the spins it converts the average precession angle to a longitudinal polarization component. Since the field after the second $\pi/2$-flipper is again longitudinal, further precession does not influence the analyzed longitudinal polarization component (the stop watch is stopped!). The analyzer consists –like the polarizer– of magnetic multilayer mirrors which only reflect neutrons of one longitudinal spin state into the detector. After ensemble averaging this means that the count rate at the detector is proportional to $(1 \pm \cos(\overline{\Psi}))/2$, [4] where $\overline{\Psi}$ is the expectation value of the angle between spin and axial direction. At the point of symmetry $J_1 = J_2 = J$ it is possible to compute the velocity difference due to an energy transfer $\hbar\omega$ and to write them as series expansion for small ω:

$$-\frac{1}{\lambda^{-1}} + \frac{1}{\lambda^{-1} + \lambda(m_n/h)\omega/2\pi} \approx -\lambda^3 \frac{m_n \omega}{h 2\pi} \tag{11}$$

the detector intensity at the symmetry point ($J_1 = J_2$) is:

$$I \;=\; \eta \frac{1}{2}\left[S(Q) + \mathcal{R}(J,\lambda) \int \cos(\underbrace{\gamma J \frac{m_n^2}{h^2 2\pi}\lambda^3}_{t} \;\; \omega) S(Q,\omega) d\omega \right] \tag{12}$$

η contains all intensity scale factors from incoming flux to detector efficiency. The underbraced product has the unit "time", the integral in Eqn. 12 represents the cos-Fourier transform of $S(Q,\omega)$ with respect to ω, the resulting function is called **intermediate scattering function,** $S(Q,t)$ [5] From Eqn. 12 it is further recognizable that the time parameter $t = \gamma J(m_n^2)/(h^2 2\pi)\lambda^3$ depends on the third power of the wavelength λ (i.e. long wavelength $\rightarrow$ very long Fourier times). In addition $t \propto J$, i.e. mainly proportional to the current through the main precession solenoids. This current usually is the parameter used to stepwise scan the Fourier time during an experiment to get a table of $S(Q,t)$ vs. t. $\mathcal{R}(J,\lambda)$ denotes the resolution effects due to differences in precession angle for different neutron paths in the beam, which lead to a dephasing of precession angles and therefore an additional loss of echo intensity. For an ideal instrument $\mathcal{R} = 1$ would hold, in reality $\mathcal{R}(J,\lambda)$ is determined by measuring a reference sample and then used for the evaluation of experiments. The information on $S(Q,t)$ according to Eqn. 12 is contained in the ratio of the intensities at the symmetry point and the average intensity $(\eta/2)\; S(Q)$. However there are practical reasons that prevent the reliable setting of the symmetry point alone. The location of the symmetry point (i.e. phase zero current in the phase coil) is extremely sensitive to tiny variations of the magnetic environment caused e.g. by displacement of larger iron parts at neighboring instruments, movement of the crane and/or thermal displacements of coils ... . Therefore the position of the symmetry point has to be measured as well as the intensity each time. In fig. 23 the minimum of single countings is indicated, intensity must be determined for 3 points $P_1 \cdots P_3$ separated by a symmetry change corresponding to

[4] The sign in front of the cosine depends on the technical realization of polarizer and analyzer (both reflecting, transmitting, one reflecting one transmitting) and on the orientation of flippers. It may be selected by choosing the signs of the flipper currents.

[5] Strictly this is only true for a $S(Q,\omega)$ that is symmetric with respect to ω. For any practical problems however this is well fulfilled since the minute energy transfers corresponding to the NSE time scale are very small compared to $k_B T$.

a quarter precession each. From these 3 values it is possible to extract the average intensity $I(Q,0)$, the echo amplitude $I(Q,t)$ and the exact symmetry point location. This also holds if any disturbance shifted the location as indicated by the three hollow circles in the figure.

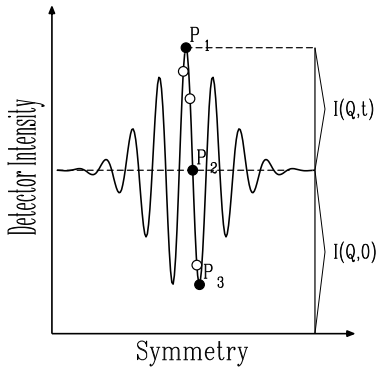

Fig. 23: *Schematic echo form, idealized.*

From the above description it follows that the NSE spectrometer measures the Fourier transform $S(Q,t)$ of the spectral part of $S(Q,\omega)$ directly. As a consequence the average count rate at the detector corresponds to half of all neutrons scattered from the sample into the solid angle of the detector (Fourier**integral**). Therefore weak spectral features are buried under the noise due to counting statistics. However the method is perfectly adapted to relaxations that are performed by most of the scattering structure. The relaxation functions are measured in the time domain directly and resolution correction consists of a division instead a deconvolution in the frequency space. One very important field for NSE investigations are "soft matter" problems. These comprise polymer melts and solutions and other complex fluids. The NSE methods opens a dynamics window in the SANS regime. Since in that regime the dynamics is determined by the balance between elastic (entropic) forces and friction and in comparison inertial forces are negligible the observed fluctuations are pure relaxations and well suited for investigation by NSE. In addition SANS scattering is coherent and usually intense compared to scattering at large angles.

The spin incoherent scattering, which frequently is the main intensity contribution in backscattering of time-of-flight spectra from organic or soft-matter samples or other hydrogen containing systems, is caused by the dependence of the scattering length on the relative orientation of nuclear and neutron spins. The fluctuating part of the scattering length due to random spin orientation contains no interference of scattering from different nuclei, i.e. the scattering intensity distributes evenly over 4π solid angle and is "diluted" accordingly. This intensity is very small compared to typical SANS intensities, in fact it is the large Q background level in SANS experiments. The dynamics of the incoherent scattering reflects the one-particle motion (self correlation). For the NSE method it is important to note that the spin-dependent scattering flips 2/3 of the neutron spins. This means that a considerable loss of polarization is encountered, only 1/3 of the neutrons contribute to the echo signal the rest is background. This 1/3 stems form the spin flipped neutrons, i.e. the echo amplitude is also inverted (negative). If coherent and incoherent scattering contributions are present this may lead to peculiar effects since the

amplitudes may cancel each other depending on their –potentially different– dynamics.

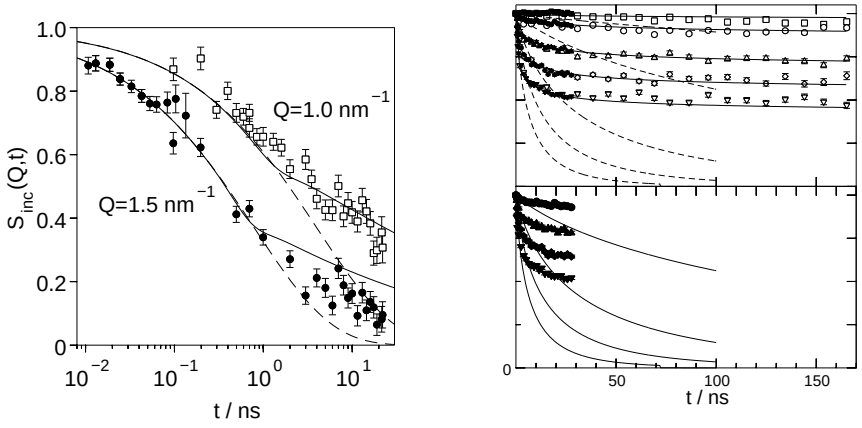

Fig. 24: *Results from neutron-spin-echo spectroscopy on polyethylene melts with height molecular weight. The left side shows the segmental diffusion at short times measured with the incoherent scattering from a protonated sample. The solid line is the expected behavior for a melt without topological constraints, the deviation at larger times indicate the first effects of a tube constraint. The right part shows plateau values where the relaxation of a chain is restricted within a virtual tube formed by the entanglements with neighbor chains. The different curves correspond to Q-values between 3 and 1.15 nm^{-1}. This experiment was done on a mixture of deuterated and protonated polymer chains. Thus the analyzed intensity corresponds to the dynamics of the single chain structure factor.*

A typical field of application for spin-echo spectroscopy is the investigation of the large scale dynamics in soft matter samples. As example figure 24 shows NSE results from a high molecular weight polyethylene melt [44]. The results reveal details of the segmental diffusion that pertain to the reptation model scenario of motion of entangled polymer chains [45]. Initially the segments diffuse without sensing the effect of other chains, at larger times the motion is hindered by topological constraints as indicated by the observation of plateaus in the $S(Q,t)/S(Q)$ decay curves [46]. These results correlate to the viscoelastic properties of polymer melts and contribute to establish a molecular explanation for their macroscopic mechanical properties.

7 Conclusion

A selection of instruments for neutron scattering has been described. The compilation cannot be complete and many further applications of thermal neutrons have been omitted, as e.g. imaging and tomography or prompt-gamma-activation analysis. Instruments at continuous sources (reactors) and those at pulsed spallation sources follow different design principles imposed by the fixed frequency pulsed nature of the spallation sources compared to the continuous ones. The common objective of the presented scattering instruments is to yield accurate data on the scattering function $S(Q,\omega)$. The variation in instrumentation originates from the variation in resolution and (Q,ω) range of interest. E.g. diffractometers integrate over ω and only structural information is obtained. Even this information is collected with different wavelength and

different angular resolution, dependent on the spatial dimensions that finally are to be probed. Inelastic instruments differ in energy resolution over a wide range of about 8 orders of magnitude spanned by the hundredths of meV range of a thermal TOF instrument down to the few neV effective resolution of a spin-echo spectrometer. A common theme for all neutron instrumentation is the optimization of intensity. This is one of the main driving forces for the variety in instrumentation. Just the necessary (and not more) resolution must be supplied in order not to reduce the available neutron flux more than necessary. Designed according to these principles a versatile and powerful suite of instruments for many purposes is found at the major neutron sources in the world. Most of these instruments are available for use by the general scientific community by application via proposal systems.

References

[1] W. Soller, Phys. Rev. **24**, 158 (1924).

[2] D. Tennant, Review of Scientific Instruments **59**, 380 (1988).

[3] J. Dash and H. Sommers, Review of Scientific Instruments **24**, 91 (1953).

[4] H. Friedrich, V. Wagner, and P. Wille, Physica B **156**, 547 (1989).

[5] E. Fermi, J. Marshall, and L. Marshall, Physical Review **72**, 193 (1947).

[6] C. Shull, Physical Review **81**, 626 (1951).

[7] C. Shull, E. Wollan, and W. Koehler, Physical Review **84**, 912 (1951).

[8] P. Boeni, Physica B: Condensed Matter **234-236**, 1038 (1997), proceedings of the First European Conference on Neutron Scattering.

[9] K. H. Andersen *et al.*, Physica B: Condensed Matter **404**, 2652 (2009), proceedings of the 7th International Workshop on Polarized Neutrons for Condensed Matter Investigations and 2nd International Symposium of Quantum Beam Science Directorate.

[10] E. Babcock *et al.*, Physica B-Condensed Matter **404**, 2655 (2009), 7th International Workshop on Polarized Neutrons for Condensed Matter Investigations/2nd International Symposium of Quantum Beam Science Directorate, Tokai, Japan, sep 01-05, 2008.

[11] G. Bruckner, A. Czermak, H. Rauch, and P. Weilhammer, Nuclear Instruments & Methods in Physics Research Section A **424**, 183 (1999), 3rd International Topical Meeting on Neutron Radiography, Luzern, Switzerland, mar 16-19, 1998.

[12] K. H. Andersen, P. M. Bentley, and L. D. Cussen, Journal of Applied Crystallography **44**, 295 (2011).

[13] T. C. Hansen *et al.*, Measurement Science and Technology **19**, 034001 (2008).

[14] H. A., H. J. P., G. O., and H. L., Zeitschrift fur Kristallographie **Proceedings 1**, 127 (2011).

[15] D. T. Bowron *et al.*, Review of Scientific Instruments **81**, (2010).

[16] H. Conrad, T. Brückel, W. Schäfer, and J. Voigt, Journal of Applied Crystallography **41**, 836 (2008).

[17] S. E. Dutton *et al.*, Journal of Physics: Condensed Matter **23**, 246005 (2011).

[18] D. Hohlwein, A. Hoser, and W. Prandl, Journal of Applied Crystallography **19**, 262 (1986).

[19] M. P. Blakeley *et al.*, Acta Crystallographica D **66**, 1198 (2010).

[20] A. J. Schultz *et al.*, Journal of Applied Crystallography **38**, 964 (2005).

[21] T. Hosoya *et al.*, Nuclear Instruments and Methods in Physics Research Section A, **600**, 217 (2009).

[22] Hammouda B., www.ncnr.nist.gov/staff/hammouda/the_SANS_toolbox.pdf .

[23] W. Schmatz, T. Springer, J. Schelten, and K. Ibel, Journal of Applied Crystallography **7**, 96 (1974).

[24] J. K. Zhao, C. Y. Gao, and D. Liu, Journal of Applied Crystallography **43**, 1068 (2010).

[25] H. Frielinghaus *et al.*, Journal of Applied Crystallography **42**, 681 (2009).

[26] E. Kentzinger *et al.*, Physica B: Condensed Matter **350**, E779 (2004), proceedings of the Third European Conference on Neutron Scattering.

[27] S. Borbely, M. Heiderich, D. Schwahn, and E. Seidl, Physica B: Condensed Matter **276-278**, 138 (2000).

[28] M. Rekveldt, Nuclear Instruments & Methods in Physics Research Section B **114**, 366 (1996).

[29] A. Radulescu *et al.*, Macromolecules **39**, 6142 (2006).

[30] M. Strobl *et al.*, Review of Scientific Instruments **82**, (2011).

[31] M. Kerscher *et al.*, Phys. Rev. E **83**, 030401 (2011).

[32] M. James *et al.*, Nuclear Instruments & Methods in Physics Research Section A **632**, 112 (2011).

[33] J. Ankner, M. Jansma, E. Blakeman, and R. Kellogg, Applied Physics A-Materials Science & Processing **74**, S1610 (2002), International Conference on Neutron Scattering, Munich, Germany, SEP 09-13, 2001.

[34] K. Mitamura *et al.*, in *Future Trends in Soft Materials Research with Advanced Light Sources*, Vol. 272 of *Journal of Physics Conference Series*, Soc Polymer Sci; Japanese Soc Synchrotron Radiat Res; Adv Softmaterial Beamline Consortium, edited by A. Takahara and K. Sakurai (IOP Publishing Ltd, Bristol, 2011), International Symposium on Future Trends in Soft Materials Research with Advanced Light Sources: Interdisciplinary of Bio- & Synthetic- Materials and Industrial Transferring, Hyogo, JAPAN, SEP 01-03, 2010.

[35] K. Lefmann *et al.*, Physica B: Condensed Matter **283**, 343 (2000).

[36] N. Tsyrulin *et al.*, Phys. Rev. B **81**, 134409 (2010).

[37] J. Ollivier, M. Plazanet, H. Schober, and J. Cook, Physica B: Condensed Matter **350**, 173 (2004), proceedings of the Third European Conference on Neutron Scattering.

[38] T. Masuda *et al.*, Phys. Rev. Lett. **96**, 047210 (2006).

[39] M. Hennig, B. Frick, and T. Seydel, Journal of Applied Crystallography **44**, 467 (2011).

[40] A. Meyer, R. Dimeo, P. Gehring, and D. Neumann, Review of Scientific Instruments **74**, 2759 (2003).

[41] E. Mamontov and K. W. Herwig, Review of Scientific Instruments **82**, (2011).

[42] *Neutron Spin Echo*, No. 128 in *Lecture Notes in Physics Vol. 128*, edited by F. Mezei (Springer, Berlin, Heidelberg, New York, 1980).

[43] M. Ohl *et al.*, Physica B-Condensed Matter **350**, 147 (2004).

[44] A. Wischnewski *et al.*, Physical Review Letters **90**, 058302 (2003).

[45] M. Doi and S. Edwards, *The Theory of Polymer Dynamics*, Vol. 73 of *International Series of Monographs on Physics* (Oxford University Press, Oxford, 1994).

[46] A. Wischnewski *et al.*, Physica B **276**, 337 (2000).